Non-linear Least Squares Fitting Technique for the Determination of Field Line Resonance Frequency in Ground Magnetometer Data: Application to Remote Sensing of Plasmaspheric Mass Density

A. Boudouridis[1,3], E. Yizengaw[1], M. B. Moldwin[2], and E. Zesta[4]

[1]Space Sciences Institute, Boulder, CO, USA, [2]Cooperative Institute for Research in Environmental Sciences, University of Colorado, Boulder, CO, USA, [3]National Center for Environmental Information, National Oceanic and Atmospheric Administration, Boulder, CO, USA, [4]The Aerospace Corporation, El Segundo, CA, USA, [5]University of Michigan, Ann Arbor, MI, USA, [6]NASA Goddard Space Flight Center, Greenbelt, MD, USA

Corresponding author: Athanasios Boudouridis (thanasis@spacescience.org)

Key Points:

- We introduce a new physics-based non-linear least squares fitting technique for the determination of Field Line Resonance (FLR) frequencies
- The new technique is based on non-linear least squares fitting of the analytical Ultra-Low Frequency resonant wave equations
- We calculate physics-based errors of FLR frequencies and the equatorial plasmaspheric mass density

Abstract

The accurate determination of the Field Line Resonance (FLR) frequency of a resonating geomagnetic field line is necessary to remotely monitor the plasmaspheric mass density during geomagnetic storms and quiet times alike. Under certain assumptions the plasmaspheric mass density at the equator is inversely proportional to the square of the FLR frequency. The most common techniques to determine the FLR frequency from ground magnetometer measurements are the amplitude ratio and phase difference techniques, both based on geomagnetic field observations at two latitudinally separated ground stations along the same magnetic meridian. Previously developed automated techniques have used statistical methods to pinpoint the FLR frequency using the amplitude ratio and phase difference calculations. We now introduce a physics-based automated technique, using non-linear least squares fitting of the ground magnetometer data to the analytical resonant wave equations, that reproduces the wave characteristics on the ground, and from those determine the FLR frequency. One of the advantages of the new technique is the estimation of physics-based errors of the FLR frequency, and as a result of the equatorial plasmaspheric mass density. We present analytical results of the new technique, and test it using data from the Inner-Magnetospheric Array for Geospace Science (iMAGS) ground magnetometer chain along the coast of Chile and the east coast of the United States. We compare the results with the results of previously published statistical automated techniques.

1 Introduction

The Earth's plasmasphere is an important plasma region of the terrestrial magnetosphere-ionosphere system, playing a significant role in the dynamics of the magnetosphere-ionosphere coupling during quiet and active periods alike (Lemaire & Gringauz, 1998; Goldstein et al., 2004; Yizengaw & Moldwin, 2005; Kotova, 2007; Darrouzet et al., 2009; Masson et al., 2009; Reinisch et al., 2009; Moldwin et al., 2016). During magnetic storms the mass loading and unloading of the plasmasphere is an integral part of the storm process, with widespread implications for a variety of processes in the magnetosphere and/or ionosphere (Sheeley et al., 2001; Yizengaw et al., 2005a). Earthward looking Extreme-UltraViolet (EUV) imagers on spacecraft high above the magnetic pole have yielded valuable information of the structure of the plasmasphere in recent decades (e.g., Goldstein, 2006; Goldstein et al., 2003, and references therein).

The equatorial plasmaspheric mass density, Peq, is a key parameter that tracks the evolution of the plasmasphere during a magnetic storm or quiet periods. A simple, cost effective technique that can measure Peq at a specific L value (and provide large scale temporal coverage), relies on the remote sensing of the plasmasphere using a pair of longitudinally aligned ground magnetometers. This method is based on the relation between the wave period, T, of a resonating magnetic field line and the mass density along this field line (Dungey, 1954), assuming theoretically determined properties of wave amplitude and phase across the latitudinal spread of the resonating bundle of fluxtubes. The standing waves on a closed magnetic field line are referred to as a Field Line Resonance (FLR). FLR frequencies belong to the Ultra-Low Frequency (ULF) range, typically in the Pc5 frequency range (1-10 mHz) within the auroral zone, and in the Pc3/4 range (7-100 mHz or periods of 10-150 s) within the sub-auroral and plasmasphere regions.

According to the Wentzel–Kramers–Brillouin (WKB) time of flight approximation in the solution of the standing wave equation (Gul'yel'mi, 1967; Kitamura & Jacobs, 1968; Schulz, 1996; Menk et al., 1999; Denton & Gallagher, 2000, and references therein), the period of the standing wave along a magnetic fluxtube is given by

$$T = 2 \int \frac{ds}{V} = n \cdot 2 \int \frac{ds}{\omega} \qquad (1)$$

where n is the wave mode number, V, the Alfvén speed, s the distance along the magnetic field line, B the magnetic field, ρ the mass density all along the field line, and μ, the permeability of free space. The mass density ρ along the field lines is usually represented as a power law decrease with radial distance R

$$\rho = \rho_{eq} \left(\frac{LR_E}{R} \right)^m \qquad (2)$$

where R is the radial distance from the center of the Earth, L is the equatorial radial distance of a fluxtube in Earth radii R_E, and m is the power law index of the density decrease along the field lines. Following Schultz (1996), and assuming a dipole magnetic field, equations (1) and (2) yield the value of the equatorial plasmaspheric mass density as

$$P_{eq} = 4.4794 \times 10^{7} \frac{\left(\sin^{3}\theta_{FLR} + 1 \right)^2}{f^2 L^3} \qquad (3)$$

$$\theta_L = \cos^{-1}\left(\sqrt{\frac{1}{L}} \right) \qquad (4)$$

$$\theta_{FLR} = \frac{(3\theta_L + \pi)(3L + 2)\sin\theta_L}{8} \qquad (5)$$

where f_{FLR} is the FLR frequency. The above equations show that knowledge of the FLR frequency can yield P_{eq} at the L value of the observing ground station.

Observations have shown that FLRs are present in the inner magnetosphere down to L values of 1.5 (Menk et al., 1994, 2000). For L values lower than that, most of the magnetic field line lies within the dense ionosphere, and thus the ULF oscillations on that field line are strongly damped. Many techniques have been developed to obtain the FLR frequency of the resonating field lines (Baransky et al., 1985, 1990; Waters et al., 1991, 1994; Pilipenko & Fedorov, 1994; Menk et al., 1999, 2000). In the current study we will use the amplitude ratio (AR), and cross-phase or phase difference (CP or PD) techniques. Both techniques rely on measurements from two adjacent ground stations, at approximately the same magnetic longitude, and separated by less than 200 km in magnetic latitude.

The techniques are described in detail in Boudouridis & Zesta (2007), and illustrated in Figure 1. Briefly, assuming a latitudinally uniform distribution of resonating field lines according to (1), the FLR frequency of the waves decreases as the field line length increases, therefore the FLR frequency is decreasing with increasing latitude (Menk et al., 1994). At every latitude, the wave amplitude exhibits a maximum at the FLR frequency of that field line (Figure 1, panel 1 from top), while the wave phase reverses, shifts by 180° (panel 2 from top) across the latitude of the resonance. For two adjacent in latitude magnetometer stations, the ratio of their wave

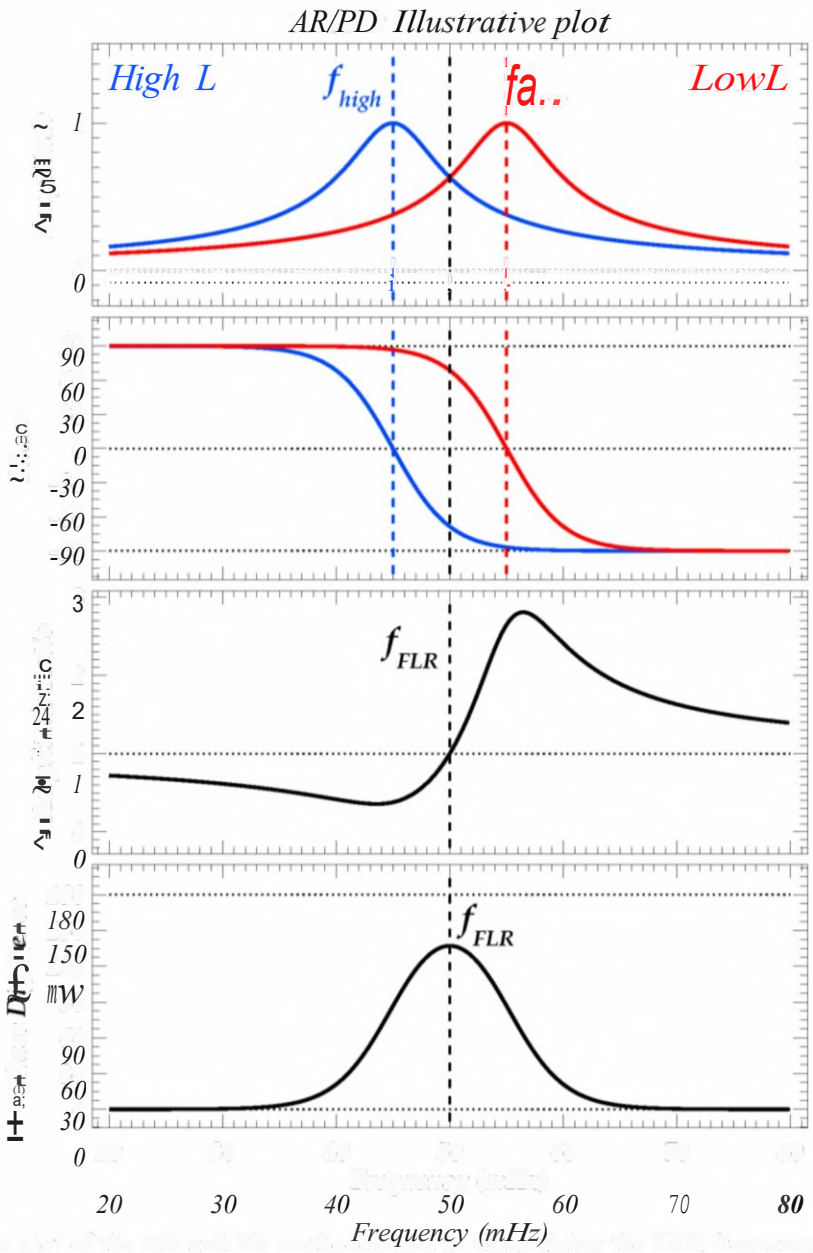

Figure 1. Illustrative plot of the AR and PD methodologies in determining the FLR frequency of the waves at the mid-point of a longitudinally aligned station pair. From top to bottom the four panels show the wave amplitude at the two stations, the wave phase, the amplitude ratio, and the phase difference.

amplitudes (AR) has a transition through 1 (panel 3 from top), while the difference of their wave phases (PD) demonstrates a maximum value (panel 4 from top), at the frequency half way between the peak amplitude frequencies of the two stations. Since for two stations in close proximity to each other the frequency decreases almost linearly with increasing latitude, the mid-point frequency is the FLR frequency at the mid-point latitude between the stations. The two frequency values, one from AR and one from PD, yield two independent measurements of the FLR frequency for the L value of the mid-point between the two stations. A chain of longitudinally aligned magnetometers can thus observe the FLR frequency at a range of L values, as many as the number of pairs of stations that can be formed between the existing stations of the chain. As the Earth rotates the chain measures the latitudinal distribution of the FLR frequency at

all magnetic local times (MLTs), as long as there are waves present in the magnetosphere. This ultimately yields the radial distribution of the equatorial plasmaspheric mass density (Chi et al., 2013).

2 Analytical FLR Determinations

The two FLR detection techniques mentioned above have been automated, using statistical methods to pinpoint the FLR frequency (Berube et al., 2003; Boudouridis & Zesta, 2007). The first steps involve generation of the dynamic spectra of the magnetic observations from the two stations, and calculation of the AR and PD for the station pair, for the frequency range around resonances, typically the Pc3/4 ULF range for the plasmasphere. Subsequent steps (detailed in Boudouridis & Zesta (2007)) include smoothing of the AR and PD in two dimensions (frequency vs time), and application of various statistical manipulations of the data, such as the t-test to estimate a meaningful maximum of the PD, or time-constant ratio of the average amplitude at two frequency ranges to estimate the transition through 1 of the AR, at the desired time step through the data. The end result is two curves, one for AR and one for PD, of derived FLR frequencies as a function of time during the period of ULF wave presence, typically in the dayside magnetosphere (Boudouridis & Zesta, 2007, their figures 2 and 3).

The statistical methods used for the FLR frequency determination yield reasonably good results whenever there is sufficient Pc3/4 ULF wave power present. This occurs mostly on the dayside magnetosphere. Despite their success in pinpointing the FLR frequency in magnetometer data from a pair of ground stations, the statistical techniques use ad hoc detection criteria that lack the robustness of a physics-based technique. The analytical, physics-based technique that we present in this paper uses the analytical standing wave equations to calculate the expected AR and PD for the station pair, and then fit them to the data at the desired time resolution. At each time step the transition through 1 of the AR, and the maximum of the PD can be calculated from the resulting analytical curves, yielding the time evolution of the FLR frequency for the two FLR determination techniques. The additional advantage of the new analytical technique is the estimation of physics-based errors of the FLR frequency and the equatorial plasmaspheric mass density.

2.1 ULF wave equations and AR/PD fitting

Following Kawano et al. (2002), the wave phase, Pow. and amplitude, H_{0W}. of a standing wave at the lower latitude station of the station pair, as a function of frequency, are given by

$$\%\% = \tan^{-1}\left(\frac{f}{a}\right) \tag{6}$$

$$Ho = \frac{b\%}{\sqrt{1+\frac{(f-b_2)^2}{b_1}}} \tag{7}$$

where f is the wave frequency, and the parameters $[at, b;]$ define the wave characteristics as follows (refer to Figure I): a, represents the phase reversal frequency, a_0 is a measure of the phase reversal rate with frequency, b represents the frequency of the peak amplitude, b, is a

measure of the amplitude change rate with frequency, and b is the peak wave amplitude. Similarly, the wave equations for the higher latitude station are given by

$$Pa = \tan^{-1}\left(\frac{f}{a,}\right) \quad (8)$$

$$H. = \frac{b,}{\sqrt{1 + (f - bs)^2}} \quad (9)$$

$$high \quad b,$$

The phase difference AP, and amplitude ratio $H,$, for the station pair are given, respectively, by equations

$$Ad = do - 9nan \quad (10)$$

$$H, = \frac{Ho}{Hnan} \quad (11)$$

This convention yields a maximum PD at the midpoint between stations, and a transition from lower to higher than 1 value for the AR at the same location, since the frequency of the standing waves decreases with increasing latitude as mentioned earlier (Menk et al., 1994). With this parameterization, equation (10) has 4 free parameters, a $(i = 0, \ldots, 33)$, and equation **(11)** has 6 free parameters, $b;$ $(i = 0, \ldots, 5)$. These free parameters can be determined by non-linear least squares fitting of the PD and AR data as a function of frequency at every step in time, using the analytical equations (6)-(11).

Figure 2 demonstrates the application of the analytical technique to a station pair located at Puerto Natales (PNT) and Punta Arenas (PAC) in Southern Chile. Comparison with the statistical results of Boudouridis & Zesta (2007) are also shown in Figure 2. Panels 1 and 3 from the top show the PD and AR of the pair for the time period 1300-1600 UT on 21 December 2003, as a function of time and frequency, color coded with the scales on the right of each panel. These are calculated from the ground magnetic field data observed at PNT and PAC. The horizontal black lines in panels 1 and 3 denote the maximum PD and AR transition through **1,** respectively, determined with the statistical methods of Boudouridis & Zesta (2007) at 1-min intervals.

Panels 2 and 4 from the top show the results of the non-linear least squares fitting of equations (10) and (11) to the observed PD and AR, respectively, for one such 1-min interval, 1348-1349 UT, denoted by the vertical white lines in panels 1 and 3. The black lines in panels 2 and 4 are the corresponding measured PD and AR (from the color-coded displays of panels 1 and 3) plotted as a function of frequency for this 1-min interval. The orange lines are the corresponding non-linear least squares fits of the black curves with the functions of equations (10) and **(11).** The red diamonds in the two panels mark the statistical PD maximum/AR transition through 1 using the methodology of Boudouridis & Zesta (2007). The blue diamonds denote the fitted PD maximum/AR transition through 1, using the new analytical technique. The vertical dashed lines and captions on the right of the panels, of the same colors, show the FLR frequencies determined with the two methods. The same procedure is applied for every minute of the interval shown, 1300-1600 UT. This yields the analytical equivalent of the statistical FLR frequency determinations (black horizontal lines) of panels 1 and 3. Figure 3, top panel, shows the statistically and analytically determined FLRs for both the PD and AR techniques at 1-min

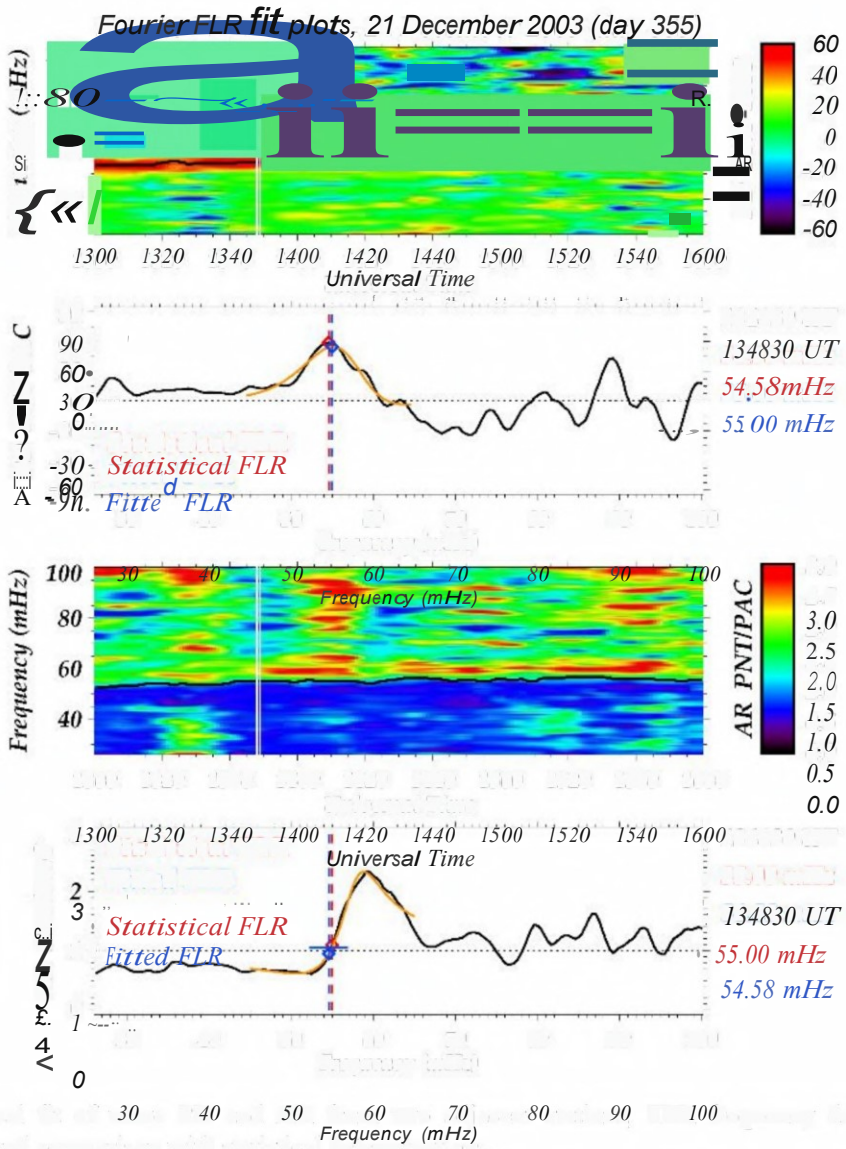

Figure 2. Analytical fit of wave PD and AR from two adjacent stations, FLR frequency determination (with estimated errors), and comparison with statistical determinations.

intervals across the same time period as in Figure 2. We discuss these results in more detail below.

2.2 FLR errors

A further advantage of the new technique is the estimation of physics-based errors of the FLR frequency, which can yield physics-based errors of the equatorial plasmaspheric mass density. These are the result of error propagation from the fitting parameter errors. Considering that the two stations are in close proximity, the change of FLR frequency with latitude between them is approximately linear. Therefore, the resulting midpoint PD and AR FLR frequencies, respectively, are given by the average of the corresponding fitted parameters that represent the FLR frequencies in equations (6)-(9)

$$f_{ro} = \frac{a_1 + a_2}{2} \qquad (12)$$

$$f_{ie} = \frac{b+b_i}{2} \quad (13)$$

The fitting parameter errors, Δa_i and Δb_i, are determined by the nonlinear least squares fitting technique. As a result, the respective errors, Δf_{pp} and Δf_{pp}, can be defined as

$$\Delta f_{ro} = \frac{\Delta a_i + \Delta a_g}{2} \quad (14)$$

$$\Delta f = \frac{\Delta b_i + \Delta b_i}{2} \quad (15)$$

The resulting errors are shown as blue horizontal bars on the fitted FLR frequencies (blue diamonds), on panels 2 and 4 from the top of Figure 2. (Note that the error of the PD technique (panel 2) is present but not visible as it is very small).

3 Plasmaspheric Mass Density

Once the FLR frequency is known, the plasmaspheric mass density can be calculated through equations (3)-(5). Equation (3) also yields the error in P_{eq} as

$$\Delta P_{eq} = \frac{-2\Delta f}{f} \quad (16)$$

where Δf is either Δf_{pp} or Δf_i from equations (14) and (15), respectively. The results for the interval 1300-1600 UT on 21 December 2003, and station pair PNT/PAC are shown in Figure 3. The top panel shows the FLR frequencies, old statistical CP (red), old statistical AR (blue), new fitted CP (black), and new fitted AR (orange). The bottom panel shows the corresponding mass density determinations in amu/cc. The errors of the new technique are shown as vertical orange bars for the AR method, and black bars for the CP method (barely visible in most instances). The FLR frequency CP error is <1% while the AR error is in the range of 10-15%. Clearly the CP method has much smaller errors. The corresponding mass density errors are 0.1-1% for the CP method, and 5-18% for the AR method.

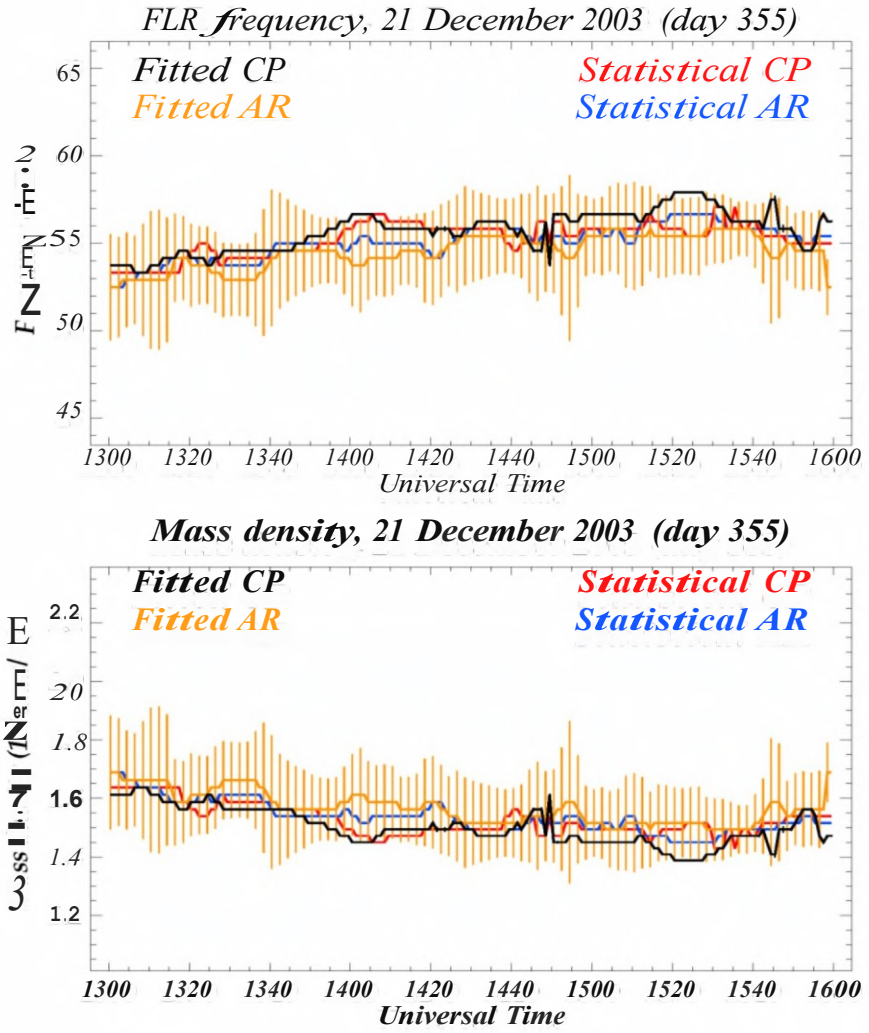

Figure 3. Application of the fit for 1300-1600 UT on 21 December 2003.

Previous methods of determining field line eigenfrequencies using pairs of ground stations result in an uncertainty in mass density of 25% or less (Berube et al., 2003). The choice of magnetic field model can lead to as large or larger uncertainties as well, especially during moderate to severe geomagnetic activity. For example, Berube et al. (2006) found the difference in density between a dipole and a Tsyganenko TOI model can be much greater than 25%. More importantly for this study, reducing the uncertainty of the FLR frequency helps constrain the composition estimates of heavy ions such as helium and oxygen. Using traditional FLR identification methods provides wide estimates of mass composition (e.g., Berube et al. (2005) found that He+/H+ ratios can range from 3% to 40% at $L = 2$ for quiet conditions). By narrowing the uncertainties of the mass density at a given L shell and geomagnetic disturbance level, the constraints on heavy ion composition can significantly improve, helping to understand ion outflow dynamics (e.g., Welling & Liemohn, 2016; Varney et al., 2016; Gkioulidou et al., 2019).

4 Application to the Halloween storms

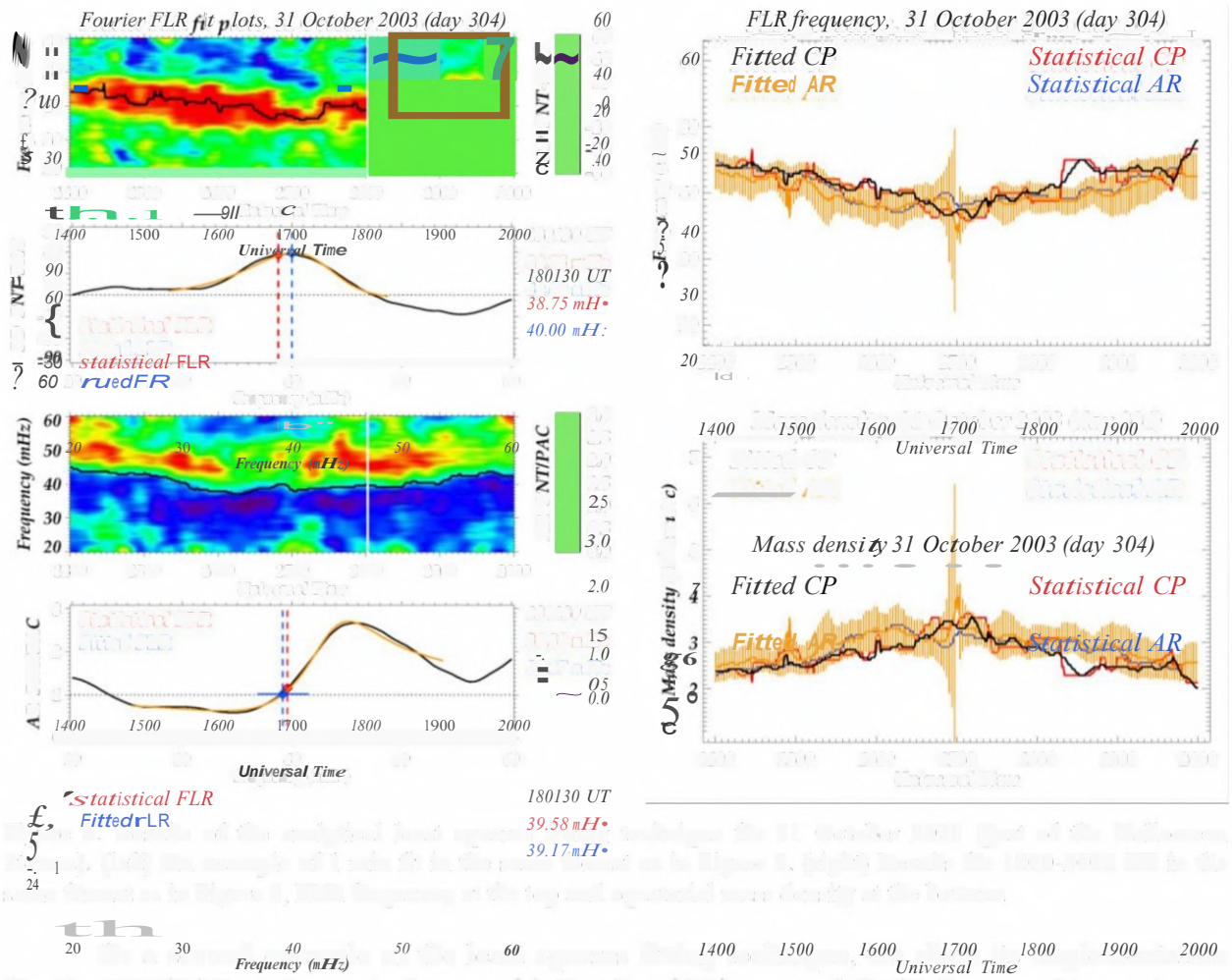

Figure 4. Results of the analytical least squares fitting technique for 31 October 2003 (part of the Halloween Storms). (left) An example of 1 min fit in the same format as in Figure 2. (right) Results for 1400-2000 UT in the same format as in Figure 3, FLR frequency at the top and equatorial mass density at the bottom.

As a second example of the least squares fitting technique, we show its implementation for the PNT/PAC station pair data on 31 October 2003, part of the Halloween Storms (e. g., Yizengaw et al., 2005b). Figure 4 shows the results for the time period 1400-2000 UT when strong ULF waves were present in the magnetosphere. On the left panel we demonstrate the application of the fit to 1 min of data during this period, in the same format as in Figure 2. The FLR frequencies during the storm are lower than the previous case, signifying higher plasmaspheric equatorial mass densities. This is clear in the plots on the right for the FLR frequency (top), and the mass density (bottom) during this storm (in the same format as in Figure 3). The FLR frequency is seen decreasing with time from ~45 mHz at 1400 UT to below 40 mHz at 1700 UT (which corresponds to noon MLT at the stations location in Chile), and returning back to 45 mHz at the end of the interval, at 2000 UT. The plasmaspheric equatorial mass density has the opposite behavior, reaching nearly 35000 amu/cc near local noon, more than twice the values observed during the 21 December 2003 example.

In terms of the least squares fitting technique performance, the results exhibit higher variability, especially for the PD technique. This is due to the much higher variability of the input PD image data. We should mention that to obtain the results of Figure 4 we applied higher image smoothing to the PD and AR images before we apply the technique. In addition, in order to achieve more stable AR fitting, we extended the fit interval around the initial guess of the FLR frequencies (b and b_2) to 14 mHz from 10 mHz that was applied in the case of Figure 2. These internal model parameters can affect the results, and eventually have to be determined

interactively for a fully automated technique, together with the initial guesses used for the a_i and b_i fitted parameters (see discussion in the following section).

The right panels of Figure 4 show that the errors of the AR technique still exhibit high variability. Close inspection of all the 1-min AR fits shows that the high errors observed are always the result of failed least squares AR fit. These abnormalities of the AR fit (and much more rarely of the PD fit) need to be addressed in a comprehensive way in the future, in order to develop a more robust and reliable technique (see additional discussion below). In this case, the PD technique errors for f_{prn} and p_a were both $\leq 1\%$. The errors for the AR technique, whenever the least squares fit converged, were $\leq 10\%$ for f_{ern} and $\leq 20\%$ for p_a.

5 Conclusions and Future Directions

In this work we described two physics-based, AR and PD, FLR frequency determination techniques. At the heart of the new methods is the non-linear least squares fitting of the AR and PD data, as opposed to statistical manipulations of this data. The analytical approach introduces physics-based errors of the FLR frequency and the equatorial plasmaspheric mass density. The results show that these errors are much smaller for the PD technique compared to the AR technique, both for the FLR frequency and the equatorial plasmaspheric mass density.

The application of the technique to the same station pair for two different days, 21 December 2003 and 31 October 2003 (part of the Halloween Storms), shows that for a fully automated technique further improvements need to be made. Some future directions are the following:

1. Introduction of criteria for the convergence or not of the non-linear least squares fitting for the two techniques, AR and PD, in order to eliminate erroneous results.
2. Use of criteria for the comparison of the AR and PD methods, in order to exclude frequencies for which the two techniques yield very different results.
3. The results of the analytical non-linear least squares fitting technique depend on the initial choice of the fit parameters a_i and b_i. This is especially true for the AR technique, but to a lesser extent for the PD technique as well. Currently these parameters are chosen manually at the beginning of the automated procedure, and are applied at every minute of the entire test interval. Instead, these parameters can be selected interactively, different at every minute of the test interval, in an effort to minimize the errors of the fit, and thus the errors of the FLR frequency and equatorial plasmaspheric mass density.
4. Internal modeling parameters, such as the extent of PD and AR image smoothing and the frequency range of the application of the least squares fitting technique, need to be determined interactively in order to achieve the best results with no user input. One way to do this is to perform the fitting for a multi-variable matrix of internal input parameters, and choose the internal parameter values that minimize a metric of the resulting FLR frequency errors.
5. Use of a more realistic magnetic field model, such as the Tsyganenko TOI model (Berube et al., 2006).
6. Devise a statistical FLR frequency model that will fill the gaps for the times when the least squares fitting technique fails, or the times when PD and AR yield results that are far apart. This could be done by building a database of FLR frequencies correlated with various solar wind and IMF parameters and/or geomagnetic indices. Then, using the statistical model based on this database, fill the gaps in FLR frequency when the technique fails with reasonable values that take into account the neighboring successful fits.

Acknowledgments, Samples, and Data

The work by Athanasios Boudouridis at the Space Science Institute (SSI) was supported by NSF awards AGS-1450512 and AGS-1848730. Mark Moldwin was supported by NSF awards AGS-1450512 and AGS-1654044. The ground magnetometer data are available at http://magnetometers.bc.edu

References

Baransky, L. N., Borovkov, Y. E., Gokhberg, M. B., Krylov, S. M., & Troitskaya, V. A. (1985). High resolution method of direct measurement of the magnetic field lines' eigenfrequencies. *Planet. Space Sci., 33,* 1369–1374.

Baransky, L. N., Belokris, S. P., Borovkov, Y. E., & Green, C. A. (1990). Two simple methods for the determination of the resonance frequencies of magnetic field lines. *Planet. Space Sci., 38,* 1573–1576.

Boudouridis, A., & Zesta, E. (2007). Comparison of Fourier and wavelet techniques in the determination of geomagnetic field line resonances. *J. Geophys. Res., 112,* A08205. https://doi.org/10.1029/2006JA011922

Berube, D., Moldwin, M. B., & Weygand, J.M. (2003). An automated method for the detection of field line resonance frequencies using ground magnetometer techniques. *J. Geophys. Res., 108(A9),* 1348. https://doi.org/10.1029/2002JA009737

Berube, D., Moldwin, M. B., Fung, S. F., & Green, J. L. (2005). A plasmaspheric mass density model and constraints on its heavy ion concentration. *J. Geophys. Res., 110,* A04212. https://doi.org/10.1029/2004JA0 10684

Berube, D., Moldwin, M. B., & Ahn, M. (2006). Computing magnetospheric mass density from field line resonances in a realistic magnetic field geometry. *J. Geophys. Res., 111,* A08206. https://doi.org/10.1029/2005JA0 11450

Chi, P. J., et al. (2013). Sounding of the plasmasphere by Mid-continent MAgnetoseismic Chain (McMAC) magnetometers. *J. Geophys. Res. Space Physics, 118,* 3077–3086. https://doi.org/10.1002/jgra.50274

Darrouzet, F., Gallagher, D. L., Andr~, N., Carpenter, D. L., Dandouras, I., D~cr~au, P. M. E., De Keyser, J., Denton, R. E., Foster, J. C., Goldstein, J., Moldwin, M. B., Reinisch, B.W., Sandel, B. R., & Tu, J. (2009). Plasmaspheric density structures and dynamics: Properties observed by the CLUSTER and IMAGE missions. *Space Sci. Rev., 145,* 55–106. https://doi.org/10.1007/s11214-008-9438-9

Denton, R. E., & Gallagher, D. L. (2000). Determining the mass density along magnetic field lines from toroidal eigenfrequencies. *J. Geophys. Res., 105,* 27,717–27,725.

Dungey, J. W. (1954). The attenuation of Alfv~n waves. *J Geophys. Res., 59(3),* 323–328. https://doi.org/10.1029/JZ059i003p00323

Gkioulidou, M., Ohtani, S., Ukhorskiy, A. Y., Mitchell, D. G., Takahashi, K., Spence, H. E., et al. (2019). Low-energy (<keV) O' ion outflow directly into the inner magnetosphere: Van Allen Probes observations. *Journal of Geophysical Research: Space Physics, 124,* 405–419. https://doi.org/10.1029/2018JA025862

Goldstein, J. (2006). Plasmasphere response: Tutorial and review of recent imaging results. *Space Sci. Rev., 124,* 203–216. https://doi.org/10.1007/s11214-006-9105-y

Goldstein, J., Spasojevi~, M., Reiff, P. H., Sandel, B. R., Forrester, W. T., Gallagher, D. L., & Reinisch, B. W. (2003). Identifying the plasmapause in IMAGE EUV data using IMAGE RPI in situ steep density gradients. *J. Geophys. Res., 108(A4),* 1147. https://doi.org/10.1029/2002JA009475

Goldstein, J., Sandel, B. R., Hairston, M. R., & Mende, S. B. (2004). Plasmapause undulation of 17 April 2002. *Geophys. Res. Lett., 31,* L15801. https://doi.org/10.1029/2004GL019959

Gul'yel'mi, A. V. (1967). Theory of hydromagnetic sounding of plasma concentration in the exosphere. *Geomagn. Aeron.,* 7, 357–363.

Kawano, H., Yumoto, K., Pilipenko, V. A., Tanaka, Y.-M., Takasaki, S., Iizima, M., & Seto M. (2002). Using two ground stations to identify magnetospheric field line eigenfrequency as a continuous function of ground latitude. *J. Geophys. Res., 107(A8),* 1202. https://doi.org/10.1029/2001JA000274

Kitamura, T., & Jacobs, J. A. (1968). Determination of the magnetospheric plasma density by the use of long-period geomagnetic micropulsations. *J. Geomagn. Geoelectr., 20,* 33–44.

Kotova, G. A. (2007). The Earth's Plasmasphere: State of Studies (a Review). *Geomagn. Aeron., 47,* 409-422.

Lemaire, J. F., & Gringauz, K. I. (1998). *The Earth's Plasmasphere.* Cambridge University Press, New York.

Masson, A., Santolik, O., Carpenter, D. L., Darrouzet, F., D~cr~au, P. M. E., El-Lemdani Mazouz, F., Green, J. L., Grimald, S., Moldwin, M. B., Nemec, F., & Sonwalkar, V. S. (2009). Advances in plasmaspheric wave research with CLUSTER and IMAGE observations. *Space Sci. Rev., 145,* 137–191. https://doi.org/10.1007/s11214-009-9508-7

Menk, F. W., Fraser, B. J., Waters, C. L., Ziesolleck, C. W. S., Feng, Q., Lee, S. H., & McNabb, P. W. (1994). Ground measurements of low latitude magnetospheric field line resonances. In *Solar Wind Sources of Magnetospheric Ultra-Low Frequency Waves, Geophys. Monogr. Ser.,* vol. 81, edited by M. J. Engebretson, K. Takahashi, and M. Scholer, pp. 299–310, AGU, Washington D. C.

Menk, F. W., Orr, D., Clilverd, M.A., Smith, A. J., Waters, C. L., Milling, D. K., & Fraser, B. J. (1999). Monitoring spatial and temporal variations in the dayside plasmasphere using geomagnetic field line resonances. *J. Geophys. Res., 104,* 19,955–19,969.

Menk, F. W., Waters, C. L., & Fraser, B. J. (2000). Field line resonances and waveguide modes at low latitudes: 1. Observations. *J. Geophys. Res., 105,* 7747–7761.

Moldwin, M. B., Zou, S., & Heine, T. (2016). The story of plumes: the development of a new conceptual framework for understanding magnetosphere and ionosphere coupling. *Ann. Geophys., 34,* 1243–1253. https://doi.org/10.5194/angeo-34-1243-2016

Pilipenko, V. A., & Fedorov, E. N. (1994). Magnetotelluric sounding of the crust and hydrodynamic monitoring of the magnetosphere with the use of ULF waves. In *Solar Wind Sources of Magnetospheric Ultra-Low Frequency Waves, Geophys. Monogr. Ser.,*

vol. 81, edited by M. J. Engebretson, K. Takahashi, and M. Scholer, pp. 283–292, AGU, Washington D. C.

Reinisch, B. W., Moldwin, M. B., Denton, R. E., Gallagher, D. L., Matsui, H., Pierrard, V., & Tu, J. (2009). Augmented empirical models of plasmaspheric density and electric field using IMAGE and CLUSTER Data. *Space Sci. Rev., 145,* 231–261. https://doi.org/10.1007/s11214-008-9481-6

Schulz, M. (1996). Eigenfrequencies of geomagnetic field lines and implications for plasma-density modeling. *J. Geophys. Res., 101,* 17,385–17,397.

Sheeley, B. W., Moldwin, M. B., Rassoul, H. K., & Anderson, R. R. (2001). An empirical plasmasphere and trough density model: CRRES observations. *J. Geophys. Res., 106,* 25,631–25,641.

Varney, R. H., Wiltberger, M., Zhang, B., Lotko, W., & Lyon, J. (2016). Influence of ion outflow in coupled geospace simulations: 1. Physics-based ion outflow model development and sensitivity study. *J. Geophys. Res. Space Physics, 121,* 9671–9687. https://doi.org/10.1002/2016JA022777

Waters, C. L., Menk, F. W., & Fraser, B. J. (1991). The resonance structure of low latitude Pc3 geomagnetic pulsations. *Geophys. Res. Lett., 18,* 2293–2296.

Waters, C. L., Menk, F. W., & Fraser, B. J. (1994). Low latitude geomagnetic field line resonance: Experiment and modeling. *J. Geophys. Res., 99,* 17,547–17,558.

Welling, D. T., & Liemohn, M. W. (2016). The ionospheric source of magnetospheric plasma is not a black box input for global models. *J. Geophys. Res. Space Physics,* 121, 5559–5565. https://doi.org/10.1002/2016JA022646

Yizengaw, E., & Moldwin, M. B. (2005). The altitude extension of the mid-latitude trough and its correlation with plasmapause position. *Geophys. Res. Lett., 32,* L09105. https://doi.org/10.1029/2005GL022854

Yizengaw, E., Wei, H., Moldwin, M. B., Galvan, D., Mandrake, L. L., Mannucci, A., & Pi, X. (2005a). The correlation between mid-latitude trough and the plasmapause. *Geophys. Res. Lett., 32,* L10102. https://doi.org/10.1029/2005GL022954

Yizengaw, E., Moldwin, M. B., Dyson, P. L., & Immel, T. J. (2005b). Southern Hemisphere ionosphere and plasmasphere response to the interplanetary shock event of 29–31 October 2003. *J. Geophys. Res., 110,* A09S30, https://doi.org/10.1029/2004JA010920

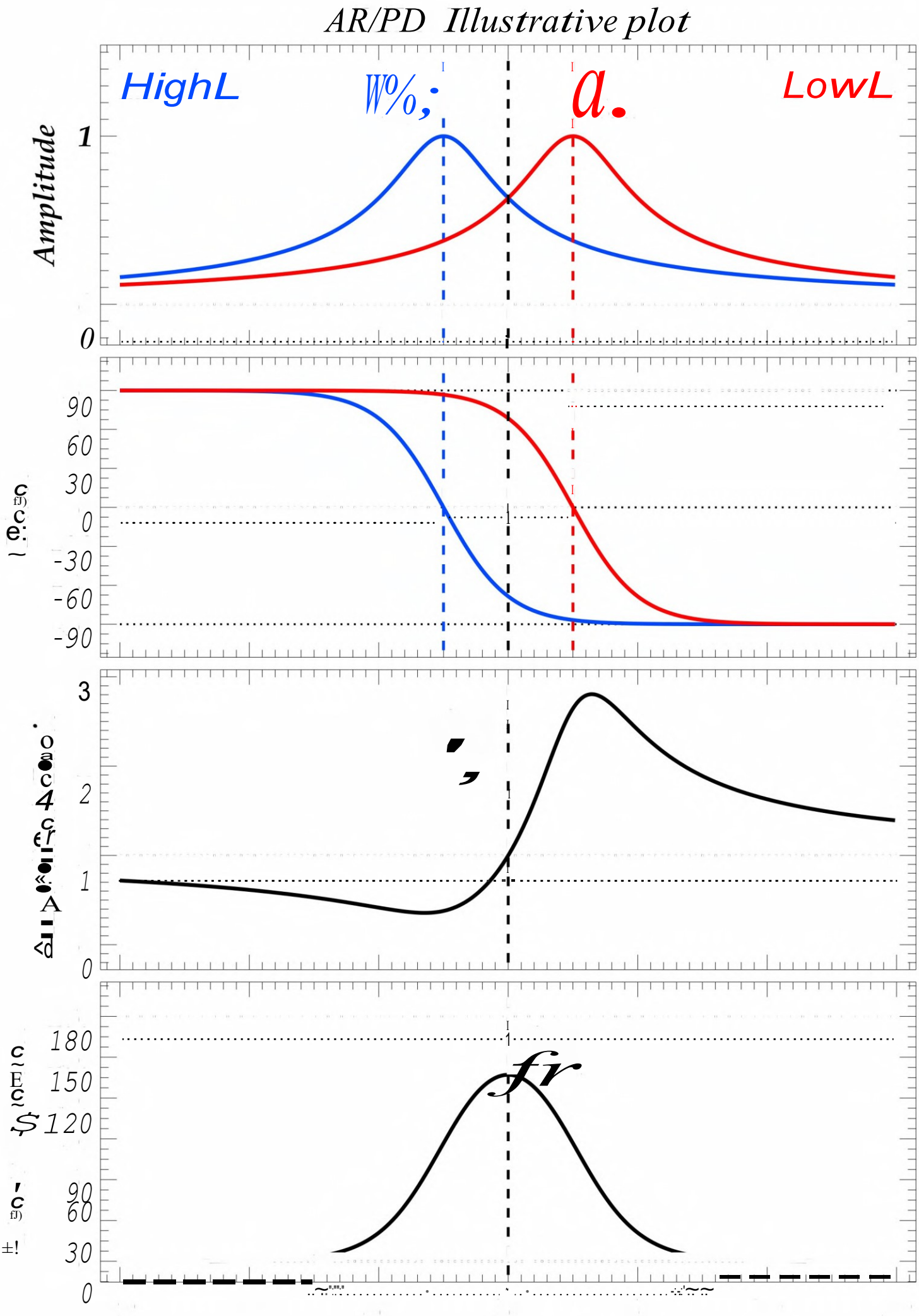
AR/PD Illustrative plot
HighL
LowL
Amplitude
1
0
90
60
30
0
-30
-60
-90
3
2
1
0
180
150
120
90
60
30
0

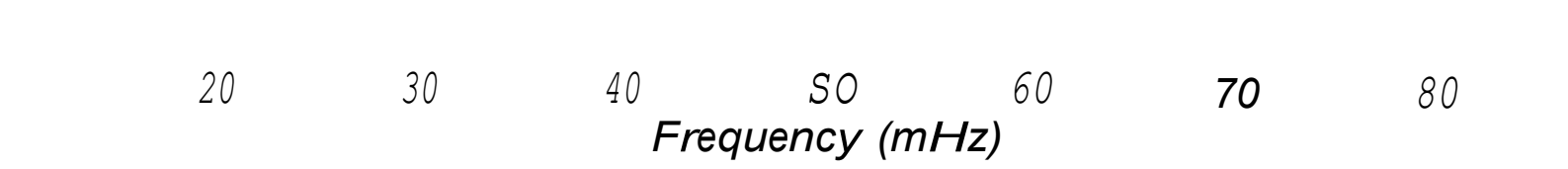
20
30
40
SO
60
70
80
Frequency (mHz)

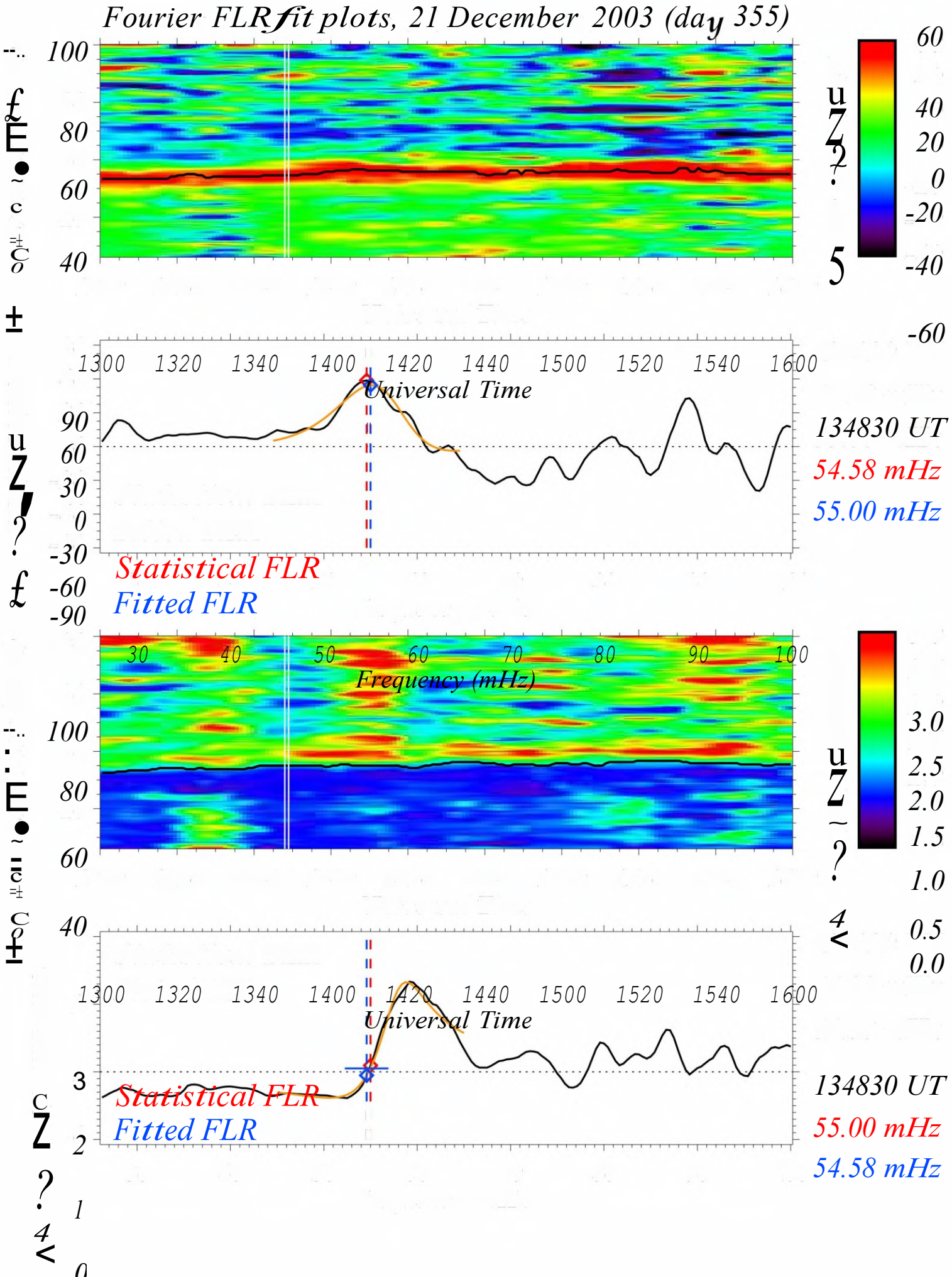
Fourier FLR fit plots, 21 December 2003 (day 355)
Universal Time
1300 1320 1340 1400 1420 1440 1500 1520 1540 1600
134830 UT
54.58 mHz
55.00 mHz
Statistical FLR
Fitted FLR
Frequency (mHz)
30 40 50 60 70 80 90 100
Universal Time
1300 1320 1340 1400 1420 1440 1500 1520 1540 1600
Statistical FLR
Fitted FLR
134830 UT
55.00 mHz
54.58 mHz

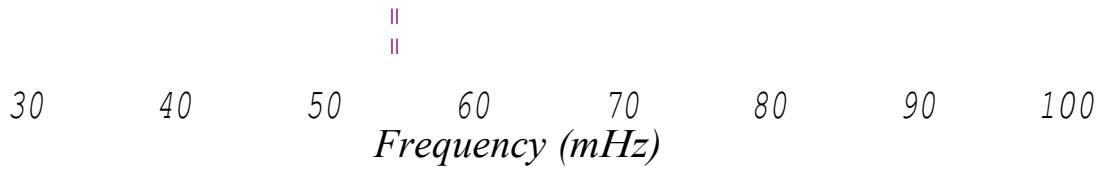
30
40
50
60
70
80
90
100
Frequency (mHz)

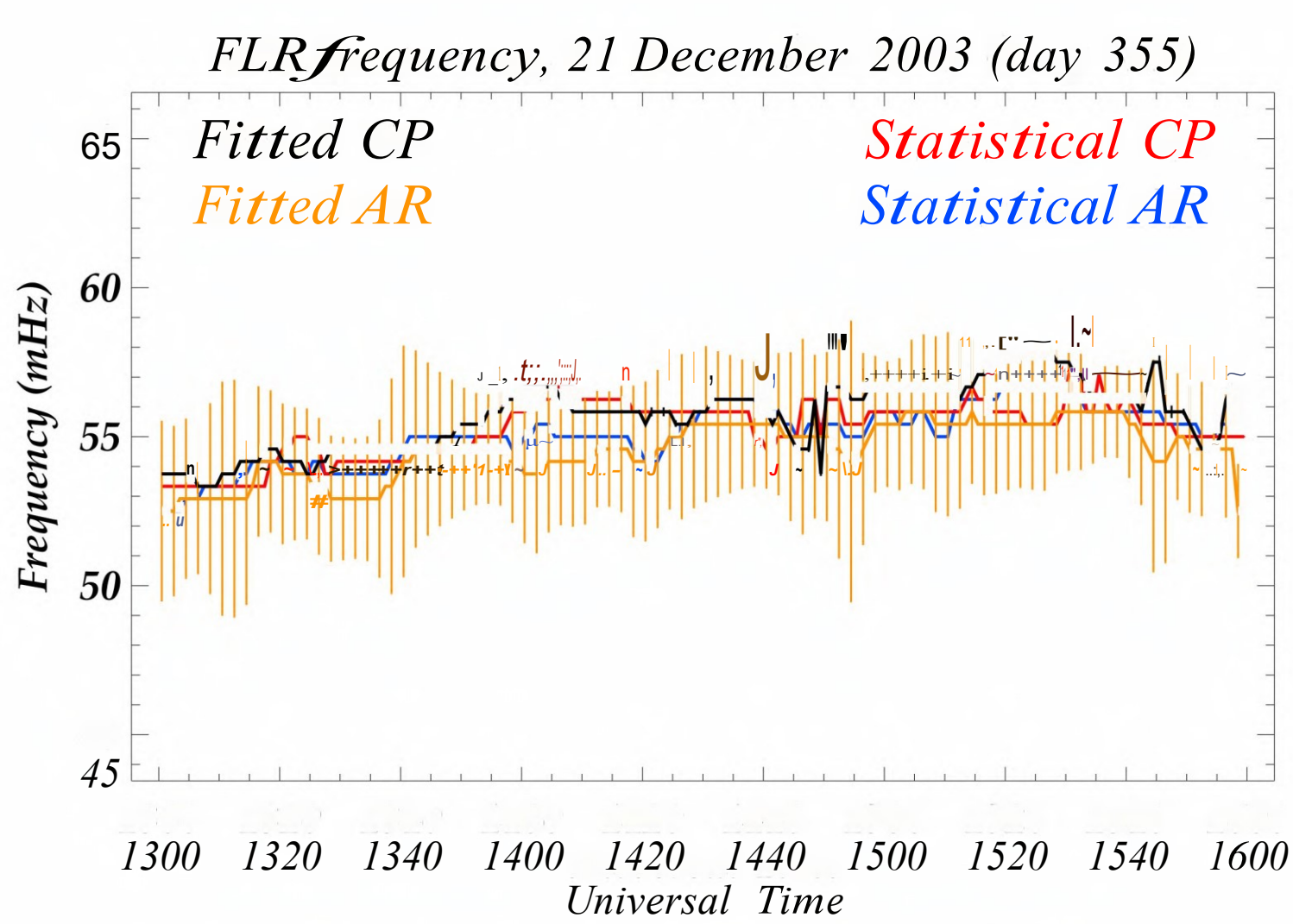
FLR frequency, 21 December 2003 (day 355)
Fitted CP
Fitted AR
Statistical CP
Statistical AR
Frequency (mHz)
65
60
55
50
45
1300
1320
1340
1400
1420
1440
1500
1520
1540
1600
Universal Time

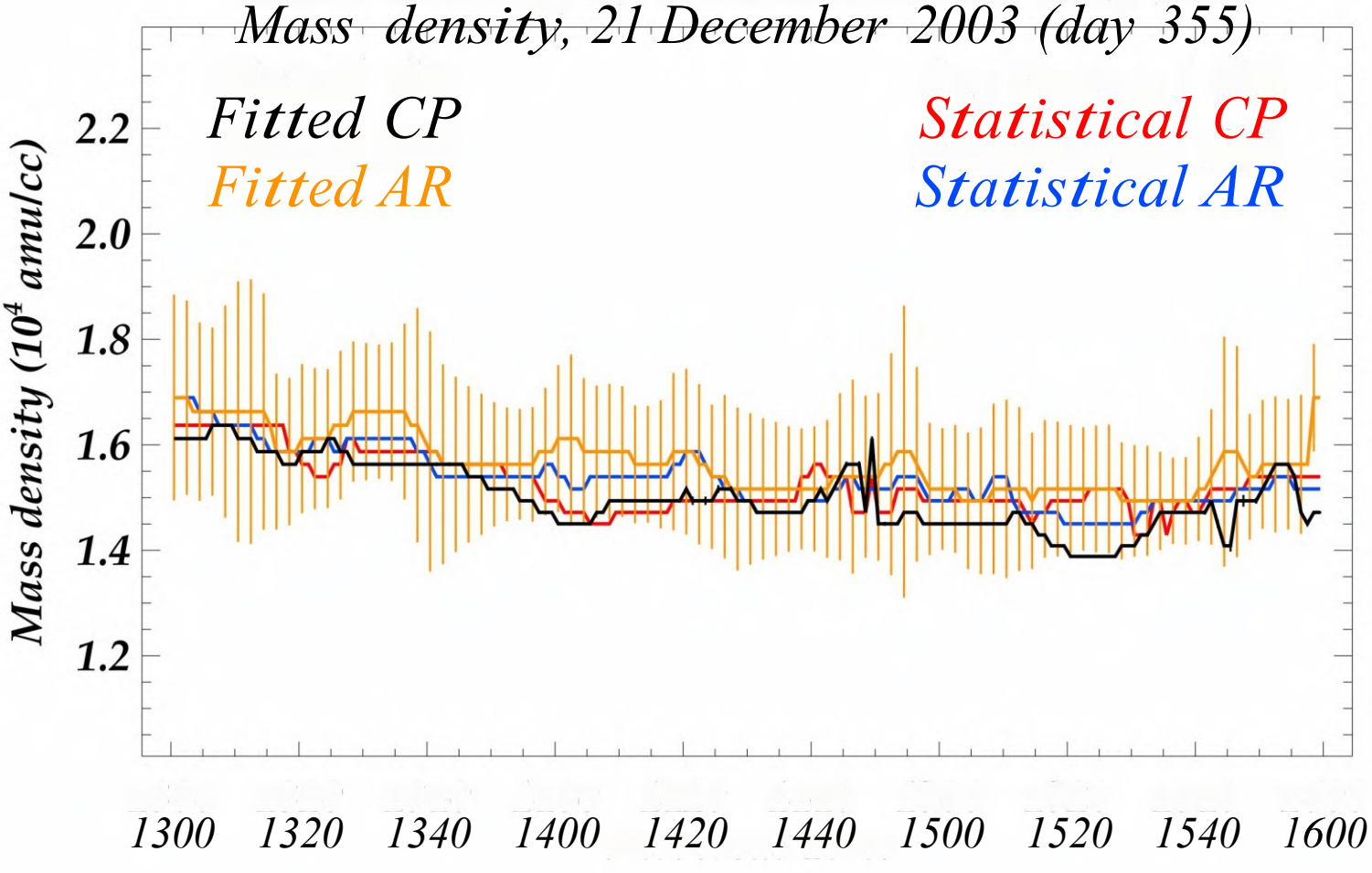
Mass density, 21 December 2003 (day 355)
Fitted CP
Fitted AR
Statistical CP
Statistical AR
Mass density (10^4 amu/cc)
2.2
2.0
1.8
1.6
1.4
1.2
1300
1320
1340
1400
1420
1440
1500
1520
1540
1600

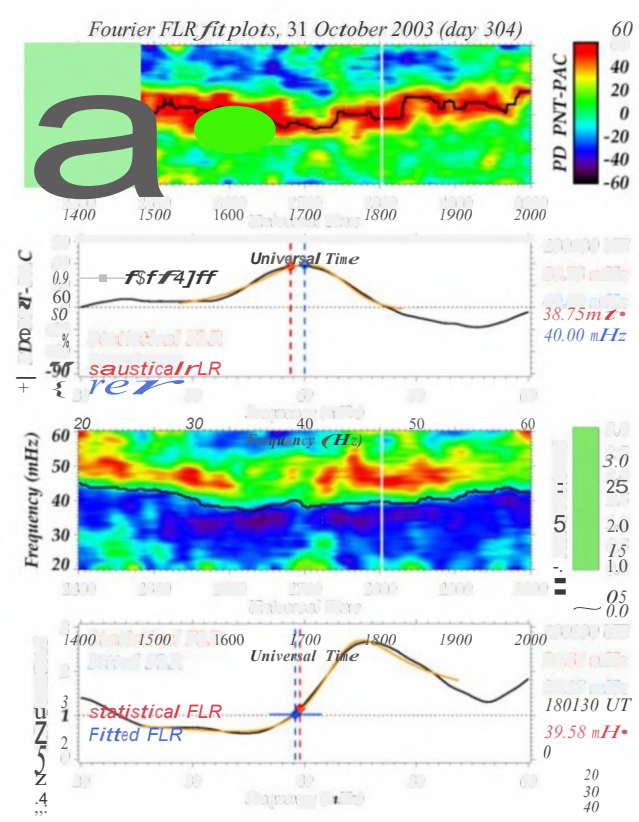
Fourier FLR fit plots, 31 October 2003 (day 304)
PD PNT-PAC
60
40
20
0
-20
-40
-60
1400
1500
1600
1700
1800
1900
2000
Universal Time
38.75 mHz
40.00 mHz
Frequency (mHz)
Frequency (Hz)
3.0
2.5
2.0
1.5
1.0
0.5
0.0
180130 UT
39.58 mHz
statistical FLR
Fitted FLR

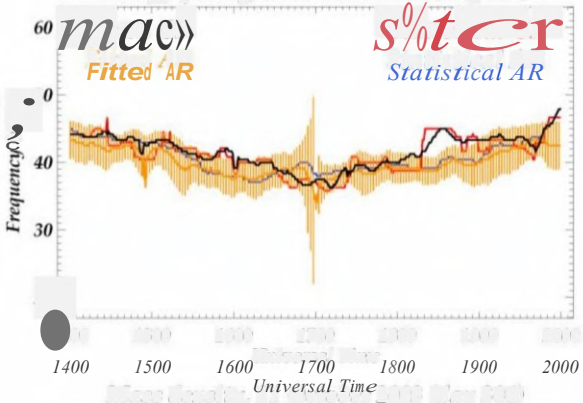
FLR frequency, 31 October 2003 (day 304)
Fitted AR
Statistical AR
Frequency (mHz)
Universal Time

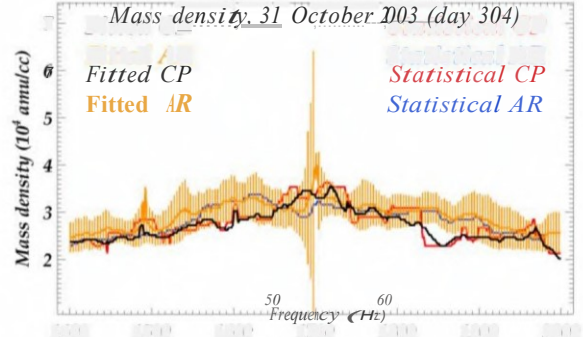
Mass density, 31 October 2003 (day 304)
Fitted CP
Fitted AR
Statistical CP
Statistical AR
Mass density (10⁴ amu/cc)
Frequency (Hz)

39.17
mH: